Electronic Supplementary Information

Critical Role of H_2 Reduction Roasting for Enhancing the Recycling of Spent Li-ion Battery Cathodes in the Subsequent Neutral Water Electrolysis

Jiayin Zhou [a], Jihong Ni [a], and Xiaofei Guan [a,*]

[a] School of Physical Science and Technology, ShanghaiTech University, Shanghai 201210, China.

* E-mail address: guanxf@shanghaitech.edu.cn

Table of Contents:

Note S1. Assembly process of the H cell for water electrolysis

The anode chamber (volume: 10 ml) and the cathode chamber (volume: 50 ml) made of borosilicate glass were connected and held together with clamps. A piece of Pt wire anode (diameter: 1 mm; Jingke Instrument, Shanghai, China) and a piece of Pt-coated Ti rod cathode (diameter: 6 mm; Yiwanlin Electronic Technology, Kunshan, China) were placed in separate chambers and immersed in the same 1 mol/L Na_2SO_4 (Macklin, 99%) aqueous electrolyte. The waste cathode powders were placed inside a removable quartz crucible (ID: 18 mm, height: 20 mm, thickness: 1 mm) in the anode chamber. Filter papers (pore size: 1~3 μm; Titan^{TM}; part No.: 02036146) were fixed at the intersection of each chamber with the cross tube to mitigate convection while allowing the transport of the metal cations.

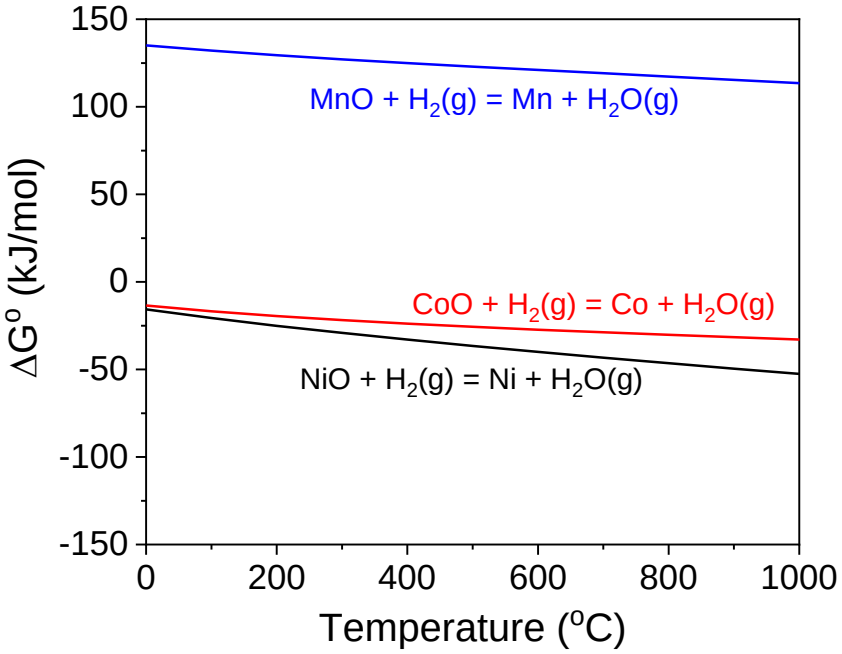

Figure S1. Standard molar Gibbs free energy change, ΔG^{o}, for the reactions: $NiO + H_2(g) = Ni + H_2O(g)$, $CoO + H_2(g) = Co + H_2O(g)$, and $MnO + H_2(g) = Mn + H_2O(g)$. The values of ΔG^{o} are obtained from HSC Chemistry Database[1].

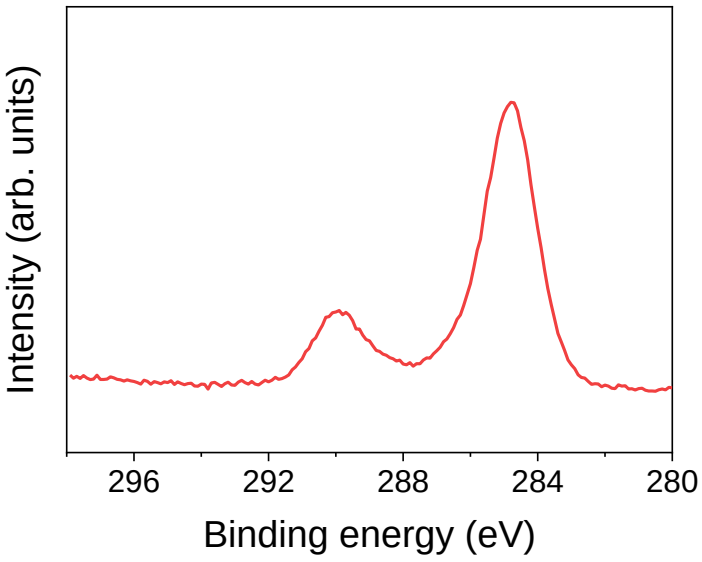

Figure S2. The high-resolution C 1*s* XPS spectrum of the roasted product that was treated in 5%H_2 at 375 ℃ for 50 minutes.

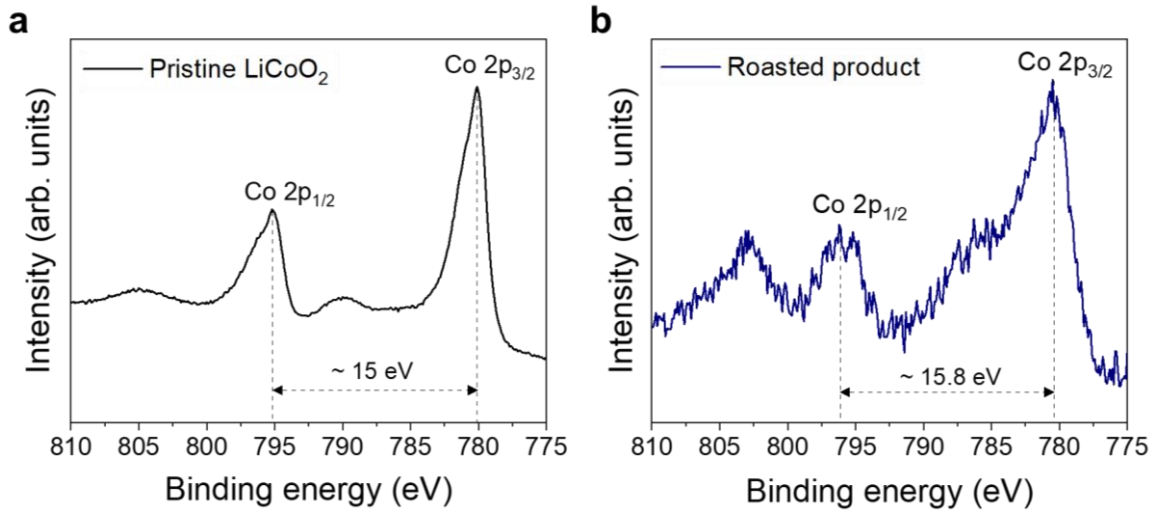

Figure S3. The high-resolution Co 2p XPS spectra of (a) the pristine waste $LiCoO_2$ powders and (b) the roasted product obtained under 375 ℃ for 50 minutes in 5%H_2.

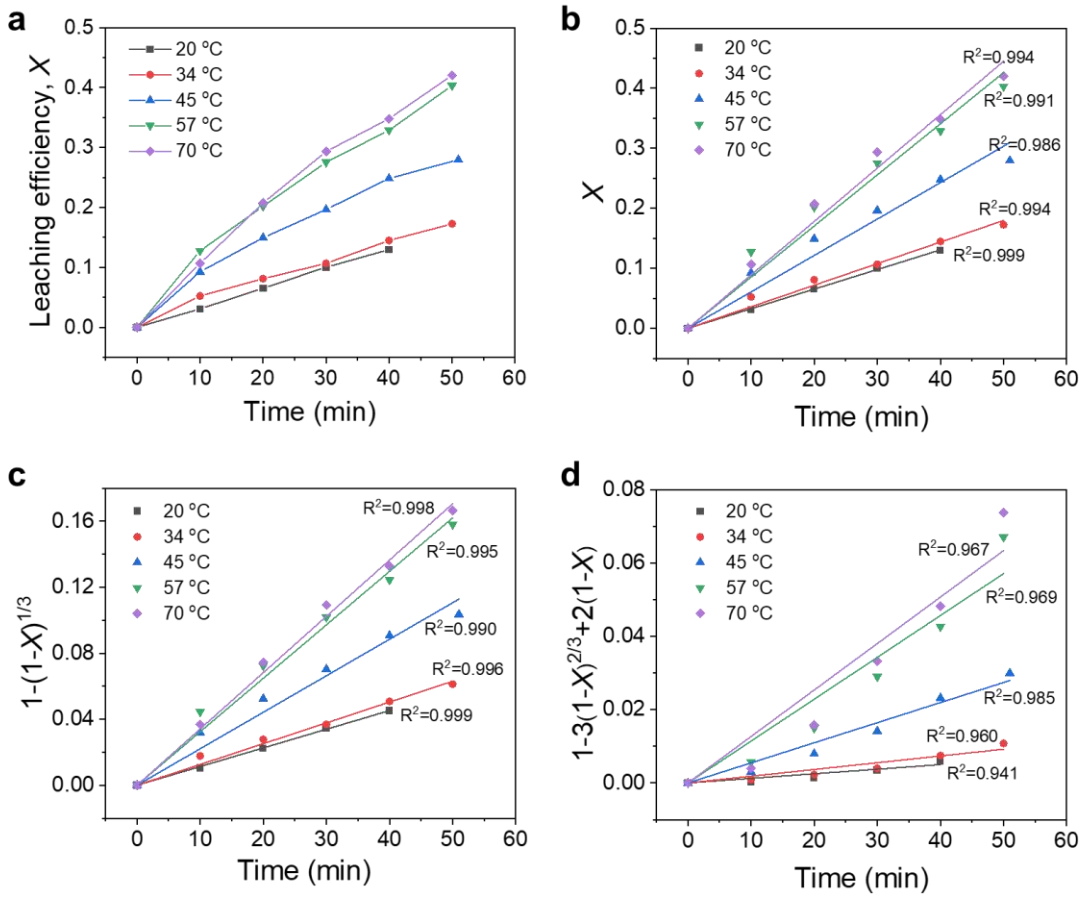

Figure S4. (a) Effects of temperature and time on the leaching efficiency of Co from the commercially purchased CoO in 0.05 mol/L H_2SO_4 solution. Kinetics analysis for the Co leaching from CoO under different reaction temperatures by (b) X vs. time, (c) $1-(1-X)^{1/3}$ vs. time, and (d) $1-3(1-X)^{2/3}+2(1-X)$ vs. time. The leaching kinetics of Co from CoO was best fit with the surface chemical reaction control model in (c), based on the coefficients of determination (R^2).

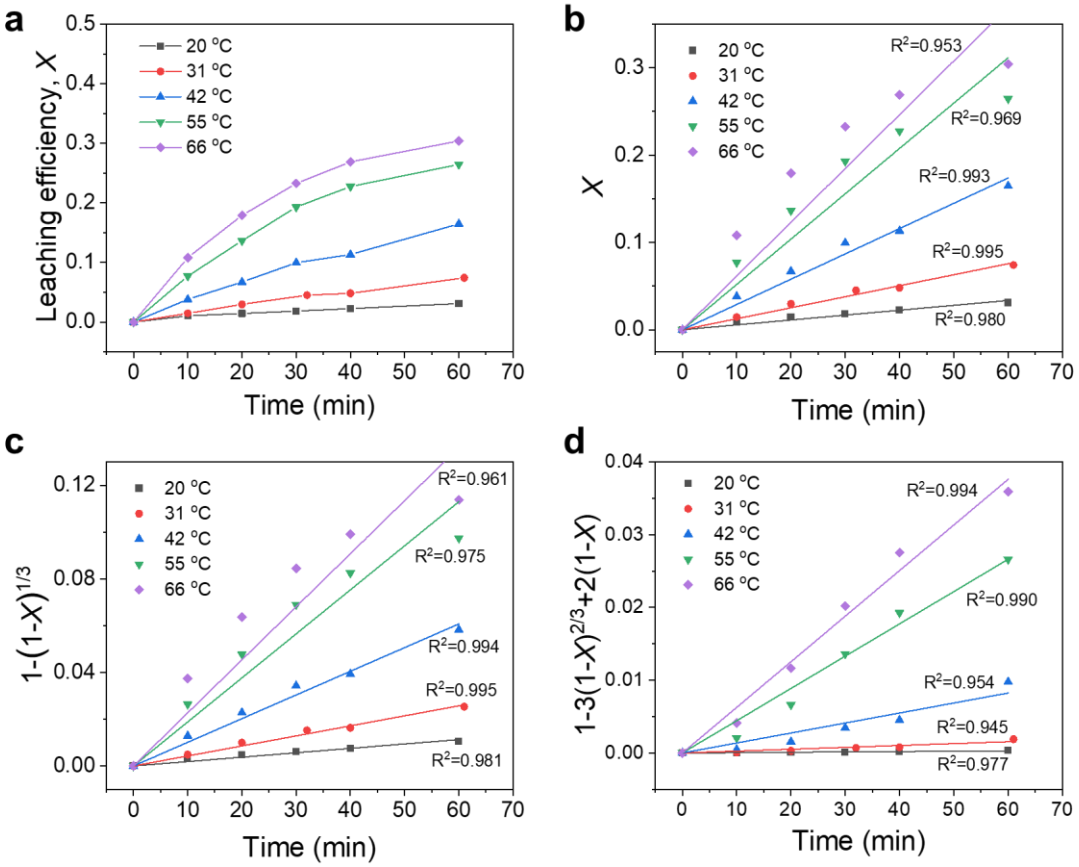

Figure S5. (a) Effects of temperature and time on the leaching efficiency of Co from the commercially purchased $LiCoO_2$ in 0.05 mol/L H_2SO_4 solution. Kinetics analysis for the Co leaching from $LiCoO_2$ under different reaction temperatures by (b) X vs. time, (c) $1-(1-X)^{1/3}$ vs. time, and (d) $1-3(1-X)^{2/3}+2(1-X)$ vs. time. The leaching kinetics of Co from $LiCoO_2$ was best fit with the residue layer diffusion control model in (d), based on the coefficients of determination (R^2).

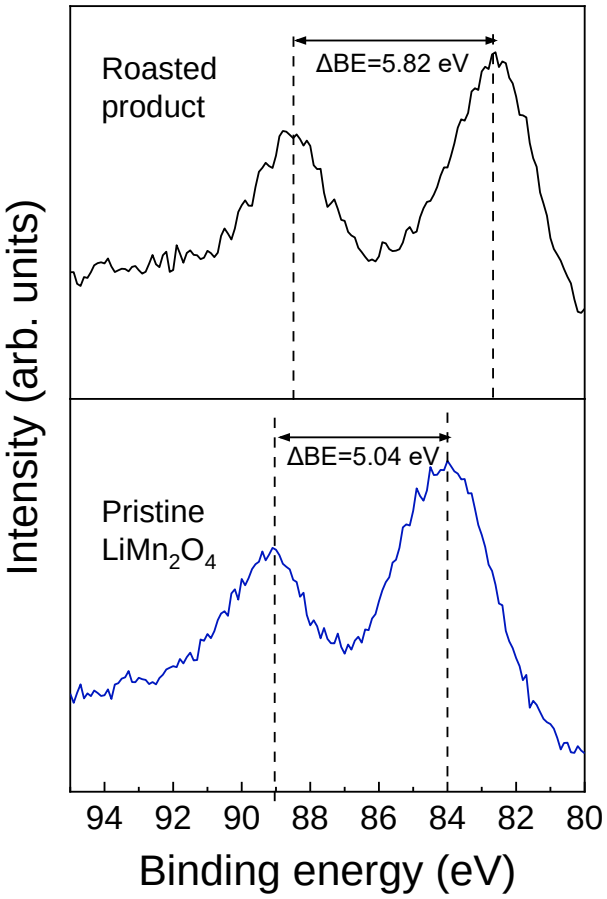

Figure S6. The core-level Mn 3*s* XPS spectra of the pristine waste $LiMn_2O_4$ and the roasted product that was treated with 5%H_2 at 850 °C for 2 hours.

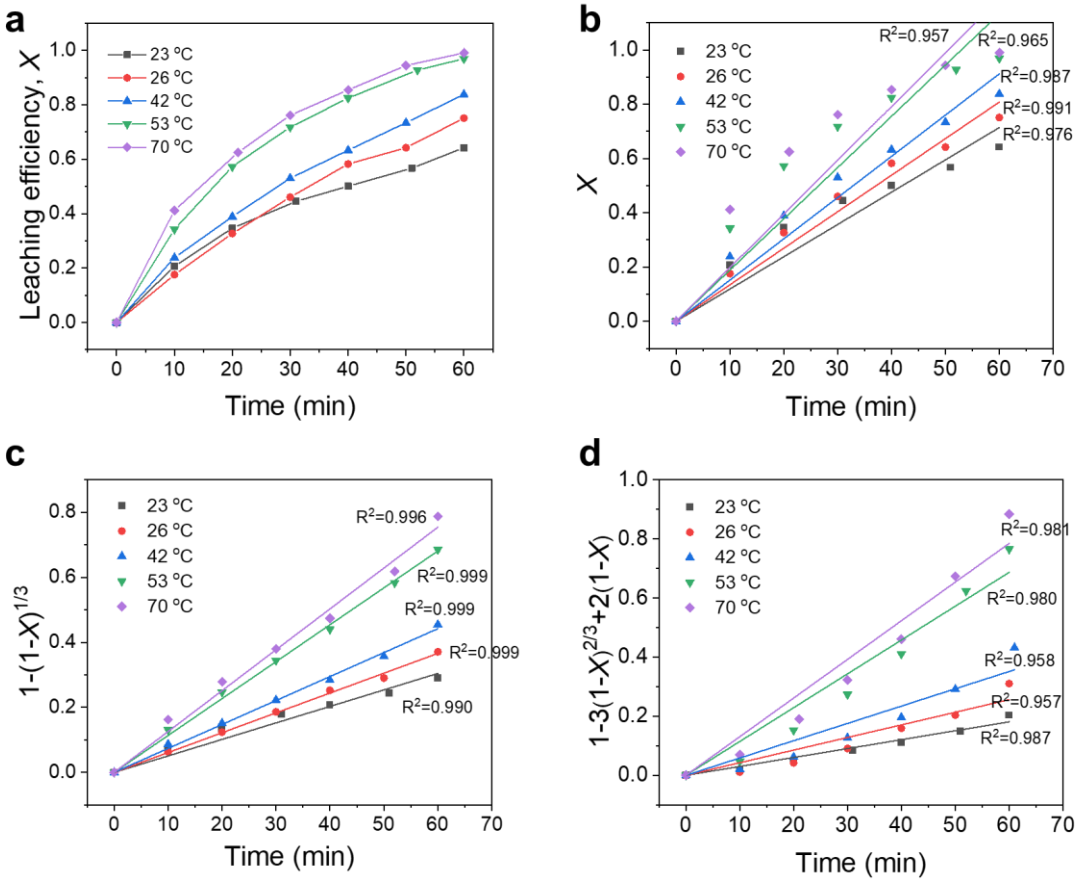

Figure S7. (a) Effect of temperature and time on the leaching efficiency of Mn from the commercially purchased MnO in 0.05 mol/L H_2SO_4 solution. Kinetics analysis for the Mn leaching from MnO under different reaction temperatures by (b) X vs. time, (c) $1-(1-X)^{1/3}$ vs. time, and (d) $1-3(1-X)^{2/3}+2(1-X)$ vs. time. The leaching kinetics of Mn from MnO was best fit with the surface chemical reaction control model in (c), based on the coefficients of determination (R^2).

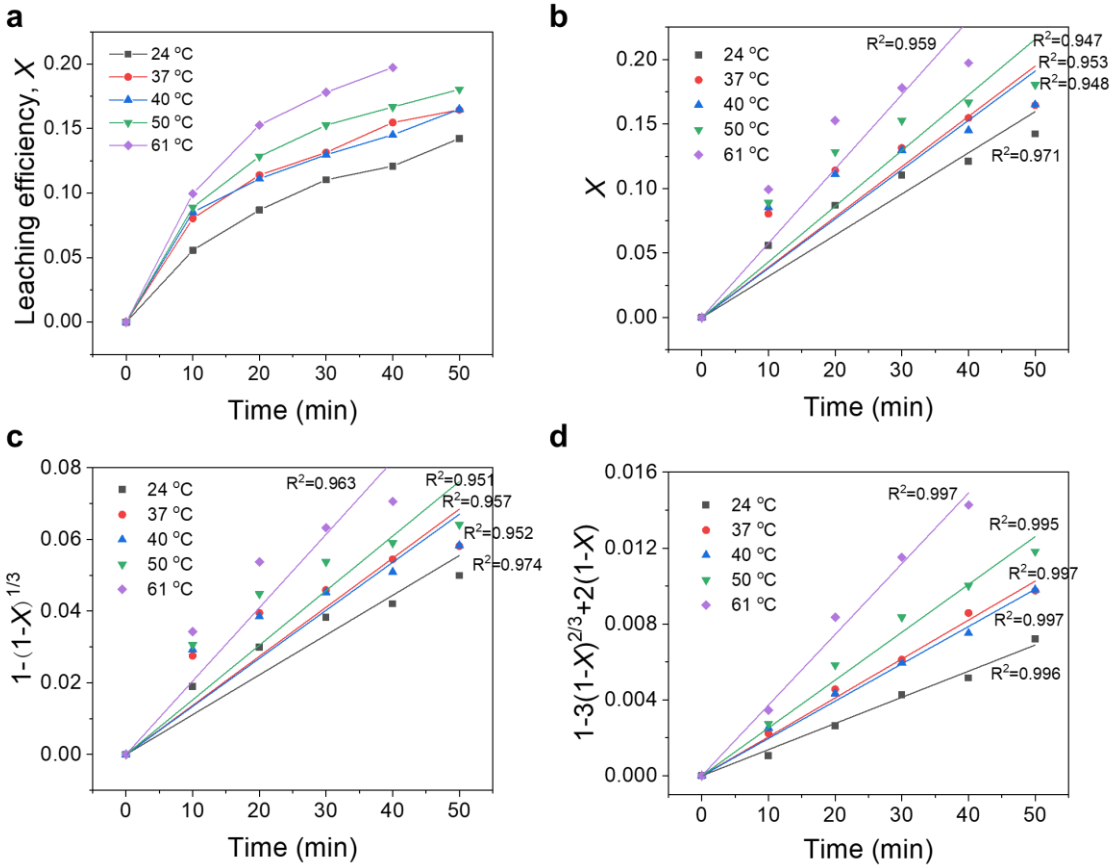

Figure S8. (a) Effect of temperature and time on the leaching efficiency of Mn from the commercially purchased $LiMn_2O_4$ in 0.05 mol/L H_2SO_4 solution. Kinetics analysis for the Mn leaching form $LiMn_2O_4$ under different reaction temperatures by (b) X vs. time, (c) $1-(1-X)^{1/3}$ vs. time, and (d) $1-3(1-X)^{2/3}+2(1-X)$ vs. time. The leaching kinetics of Mn from $LiMn_2O_4$ was best fit with the residue layer diffusion control model in (d), based on the coefficients of determination (R^2).

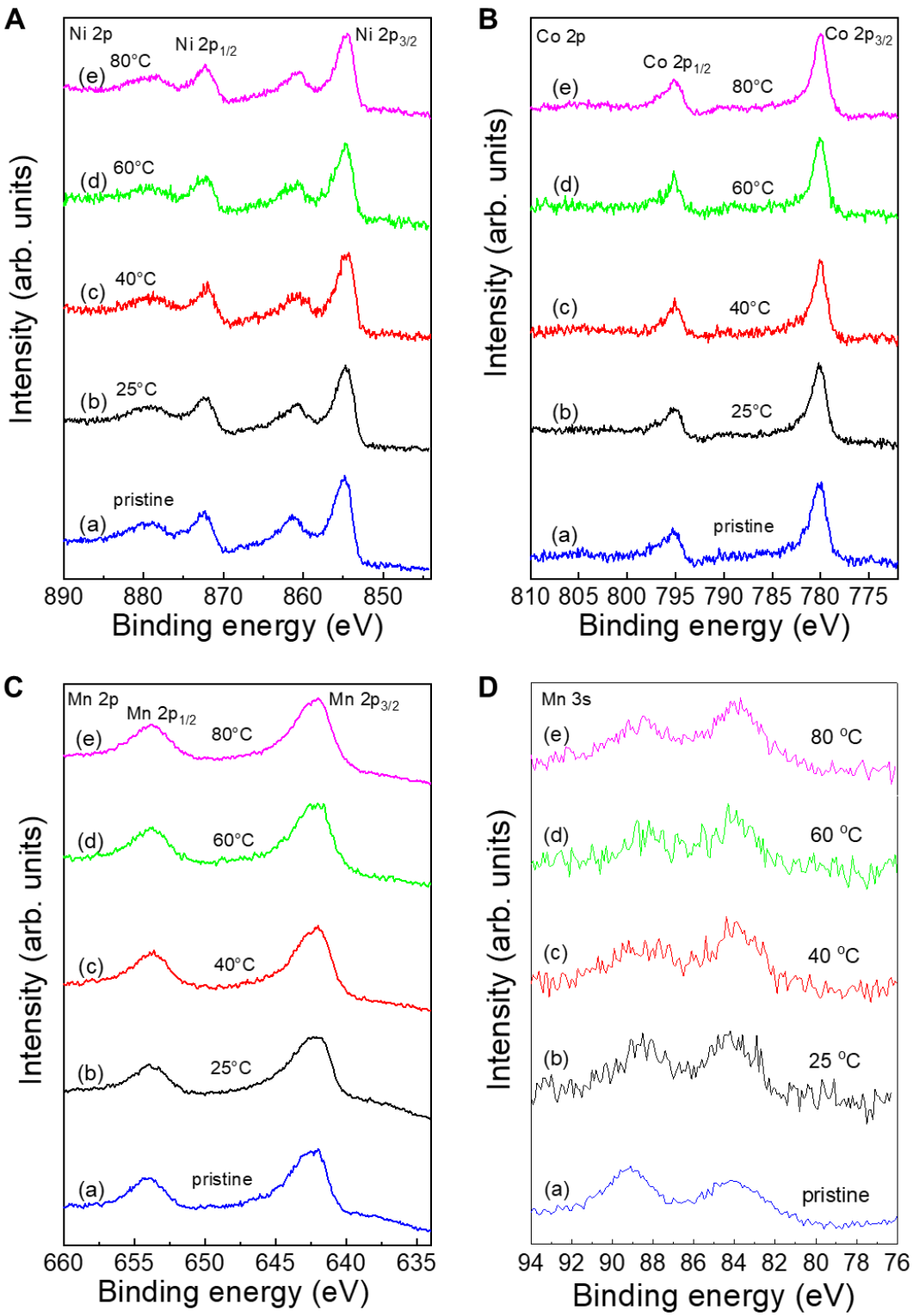

Figure S9. The high-resolution (A) Ni 2*p*, (B) Co 2*p*, (C) Mn 2*p*, and (D) Mn 3*s* XPS spectra of (a) the pristine waste NCM powders and the residue powders after leaching at (b) 25 °C, (c) 40 °C, (d) 60 °C and (e) 80 °C in the anode chambers.

Table S1. The concentrations of oxygen species (O^{2-}, O^{-}, and surface adsorbed oxygen) in pristine waste NCM powders and the residue powders after electrolysis experiments performed at different temperatures (25, 40, 60, and 80 °C). The O^{-}/O^{2-} ratio increased with the operation temperature.

	O^{2-} conc.	**O^{-} conc.**	**Surface oxygen conc.**	**O^{-}/O^{2-} ratio**
pristine	0.61	0	0.39	0
25 °C	0.50	0.41	0.09	0.81
40 °C	0.49	0.42	0.09	0.86
60 °C	0.46	0.46	0.08	1
80 °C	0.43	0.48	0.09	1.11

Note S2. Effect of applied voltage and duration on the leaching efficiency of Li, Ni, Co and Mn from waste NCM523 powders.

Figure S10 shows the leaching efficiencies of Li, Ni, Co and Mn at the same temperature (90 °C) and solid-to-liquid ratio (10 g/L) under different applied voltages (3 V and 3.5 V) for varying periods of time (12, 24, 36 and 48 hours). Due to the increase of H^+ concentration caused by larger electrolysis current and higher applied voltage, the leaching efficiency of these four elements under 3.5 V were all larger than that under 3 V, and increased with the increase of leaching time. After 48 hours, the leaching efficiency of Li reached nearly 100% under both 3 V and 3.5 V. The leaching efficiency of Ni and Co was significantly affected by the concentration of H^+ in the anode chamber. After 48 hours, the leaching efficiency of Co increased from 54.8% under 3 V to 94.8% under 3.5 V, while the leaching efficiency of Ni increased from 80.6% under 3 V to nearly 100%. Applied voltage and leaching time had less impact on the leaching efficiency of Mn, which increased from 25.7% to 48.5% under 3 V and from 38.3% to 61.2% under 3.5 V after 48 hours. Mn was more difficult to leach than Ni and Co. The leaching efficiency of Mn reached only 61.2% even under the conditions of 3.5 V after 48 h, due to the high stability of Mn-O bond[2]. In order to further improve the leaching efficiency, the use of reducing agent is necessary. The amount of residual powders in these series of experiments were too small for XRD and XPS characterization.

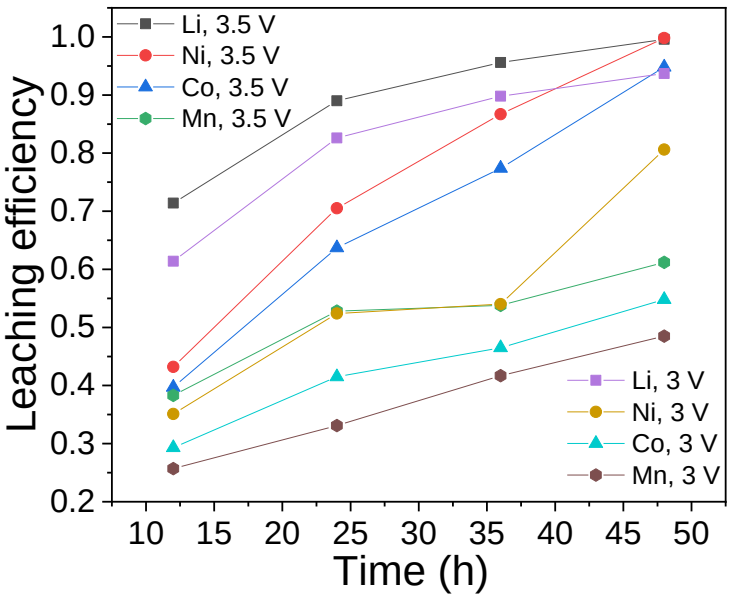

Figure S10. The leaching efficiencies of Li, Co, Ni and Mn from the waste NCM523 powders after electrolysis at 3 or 3.5 V for varying periods of time (12, 24, 36, and 48 hours) with a solid-to-liquid ratio of 10 g/L.

Note S3. Effect of solid-to-liquid ratio on the leaching efficiency of Li, Ni, Co and Mn from waste NCM523 powders.

Electrolysis experiments with different solid-to-liquid ratios (10 and 20 g/L) were performed under 90 °C for different time (12, 24, 36 and 48 hours) at 3.5 V. Figure S11 shows the effects of solid-to-liquid ratio and leaching time on the leaching efficiency of Li, Ni, Co and Mn. The leaching efficiency of the four elements all increased with the increase of the leaching time and the decrease of solid-to-liquid ratio. Similar to the effect of voltage, the effect of solid-to-liquid ratio on the leaching efficiency of Ni and Co was larger than that on Mn. After 48 hours of leaching, the leaching efficiency of Ni decreased from nearly 100 % of 10 g/L to 87.7 % of 20 g/L, the leaching efficiency of Co decreased from 94.8 % of 10 g/L to 81.3 % of 20 g/L, while the leaching efficiency of Mn decreased from 61.2 % of 10 g/L to 55 % of 20 g/L. The effect of solid-to-liquid ratio on Li leaching was small, reaching nearly 100 % after 48 hours under both solid-to-liquid ratios.

After the leaching experiment, the residual powders in the anode chamber were also characterized by XRD (Figure S12). The residual powders with a solid liquid of 20 g/L were chosen because of larger amount. After 12, 24 and 36 hours of leaching, the remaining powders again retained α-$NaFeO_2$ structure. Both the (006)/(012) peaks and (018)/(110) peaks were also found to be overlapping, indicating that the integrity of the layer structure was damaged. The two peaks at 18°-20° also proved the ion exchange between Li^+ and H^+. The intensity of diffraction peaks at higher 2θ increased with the increase of leaching time, indicating the increasing degree of ion exchange of Li^+ by H^+. It was noted that (003) diffraction peak first shifted to higher 2θ after 12 hours of leaching, and then shifted to lower 2θ after 24 and 36 hours of leaching. It was because that after 12 hours of leaching, the lattice parameters of c-axis direction first decreased, which was also due to the reduction of the distance between metal-oxygen octahedral layer caused by the reduction of electrostatic attraction between oxygen anion after Ni^{2+} migrated to the vacancies created by Li^+ removal. While after 24 and 36 hours of leaching, the distance between metal-oxygen octahedral layer increased with increase of leaching efficiency of Ni^{2+} and Li^+, which caused the increase of electrostatic repulsion of oxygen anion. As a result, the lattice parameters of the c-axis were larger, and the peak of the (003) diffraction peak shifted to the lower 2θ value. The

components of residual powder after 48 hours of leaching was the most complex. Figure S8 shows that the α-$NaFeO_2$ structure was almost totally destroyed and a new birnessite-type phase was formed. This new phase was monoclinic layered structure with the $Mn_x^{z+}O_y$ layers and the intercalated alkali metal ions and water molecules. This phase may be formed by the reaction between leached Mn^{2+} in the solution and high valence state Mn on the solid surface[3]. In addition to the birnessite-type phase, the diffraction peaks of γ-MnO_2 were also observed. A portion of the γ-MnO_2 was converted from the phase of birnessite-type phase[3].

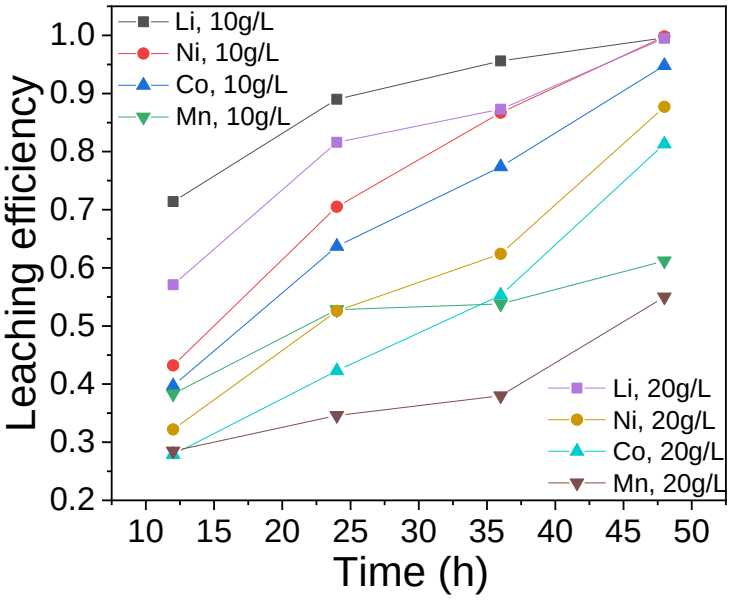

Figure S11. The leaching efficiencies of Li, Co, Ni and Mn after electrolysis at 3.5 V for varying periods of time with different solid-to-liquid ratios (10 and 20 g/L).

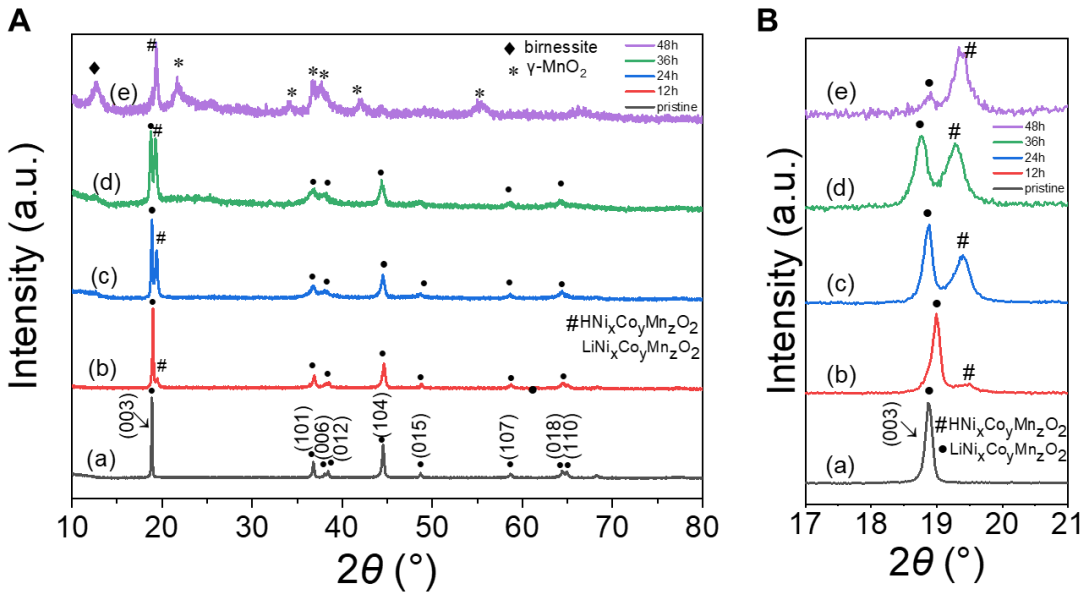

Figure S12. (A) The XRD patterns of (a) the pristine waste NCM523 powders and (b-e) the residue powders after leaching for different periods of time in the anode chambers of the electrolysis cells at 3.5 V and 90 ℃. Solid-liquid ratio: 20 g/L. (B) Magnified XRD pattern from 2θ=17° to 21°.

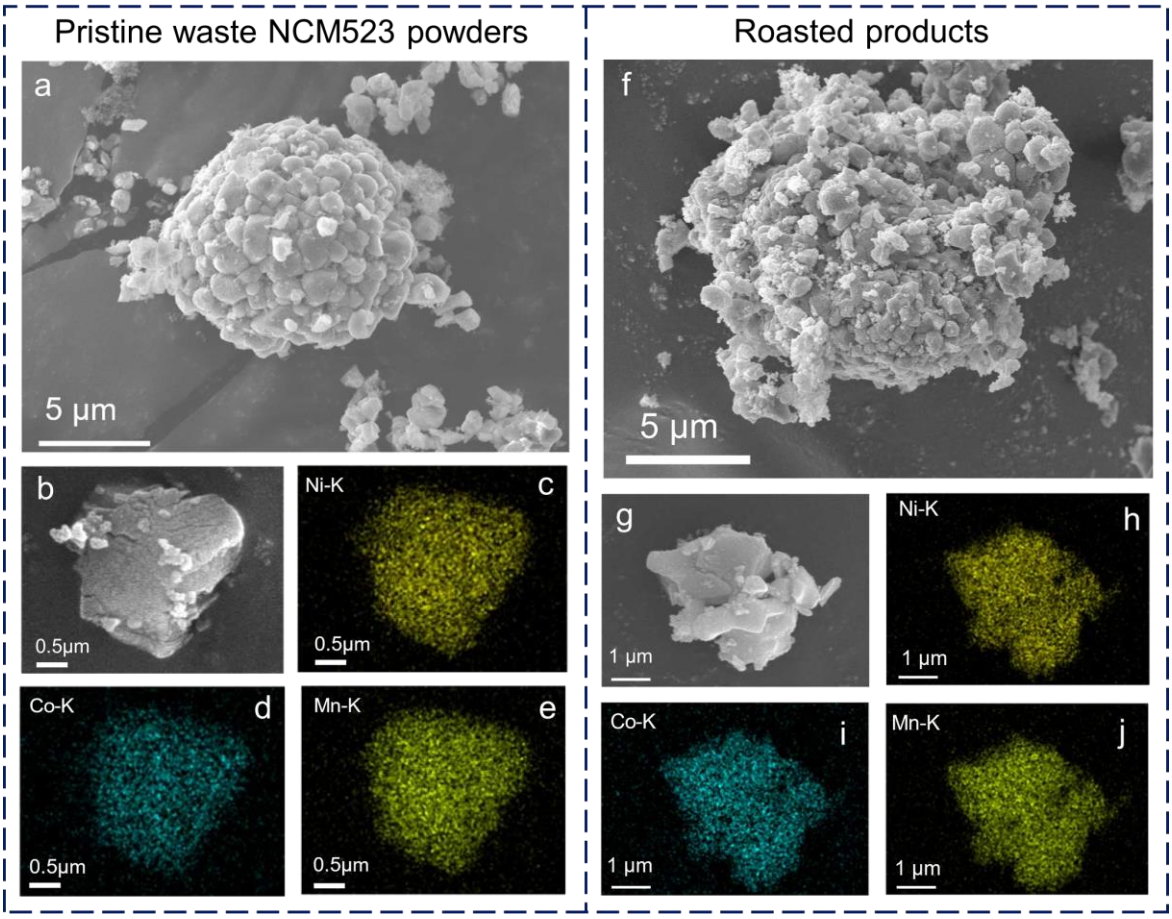

Figure S13. (a) SEM image of the pristine waste NCM523 powders. Representative EDS mapping results of (b) a pristine waste NCM523 sample for (c) Ni, (d) Co, and (e) Mn. (f) SEM image of the products that were roasted under 300 ℃ for 135 minutes in 5%H_2. Representative EDS mapping results of (g) a roasted sample for (h) Ni, (i) Co, and (j) Mn.

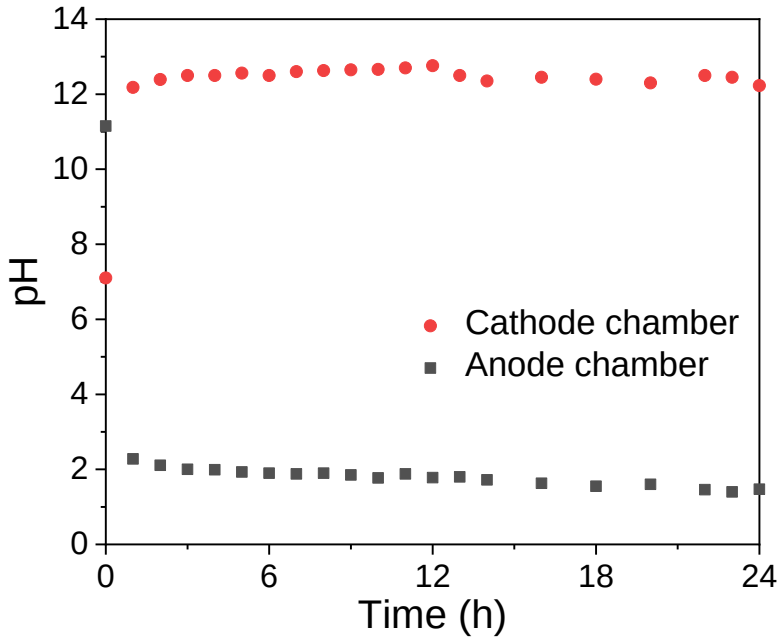

Figure S14. The time dependence of the pH values in the anode and cathode chambers of the H-cell under 3.5 V and a solid-to-liquid ratio of 10 g/L at 90 °C.

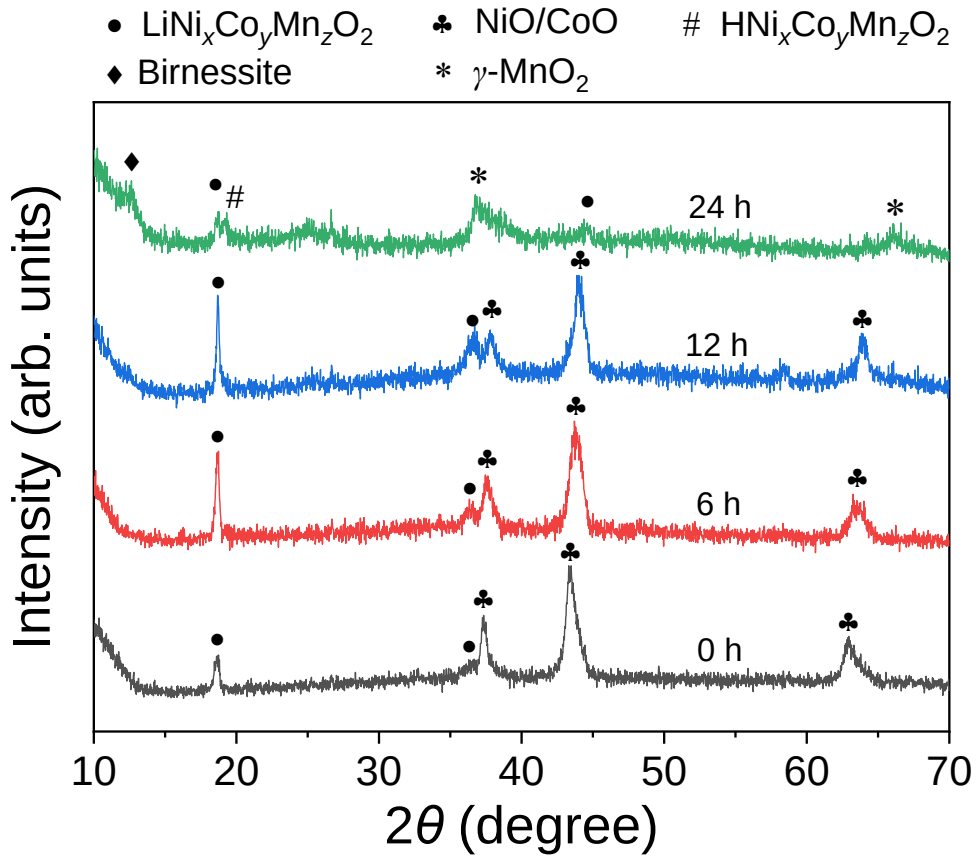

Figure S15. The XRD patterns for the roasted products (labeled with 0 h) and the residues after leaching for various periods of time (6,12, and 24 h) in the anode chamber of the H-cell.

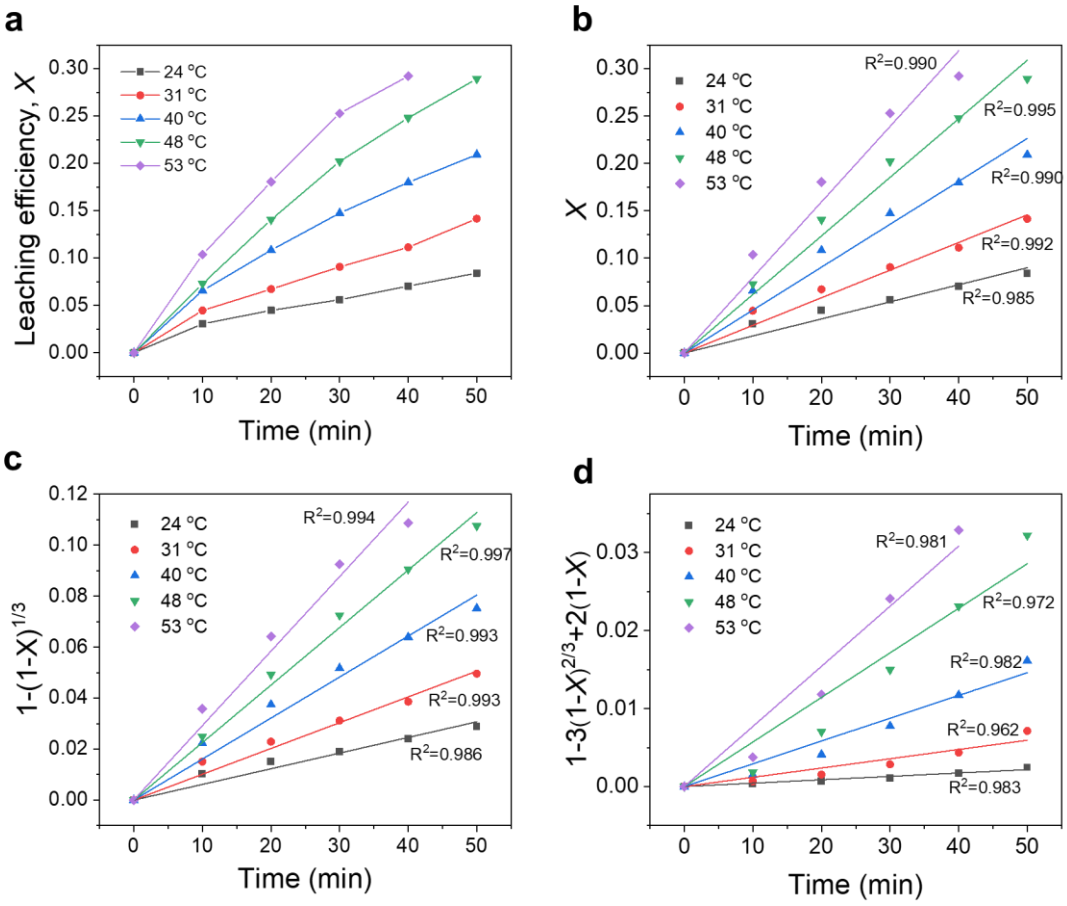

Figure S16. (a) Effects of temperature and time on the leaching efficiency of Co from the commercially purchased NCM523 in 0.05 mol/L H_2SO_4 solution. Kinetics analysis for the Co leaching from NCM523 under different reaction temperatures by (b) X vs. time, (c) $1-(1-X)^{1/3}$ vs. time, and (d) $1-3(1-X)^{2/3}+2(1-X)$ vs. time. The leaching kinetics of Co from NCM523 was best fit with the surface chemical reaction control model in (c), based on the coefficients of determination (R^2).

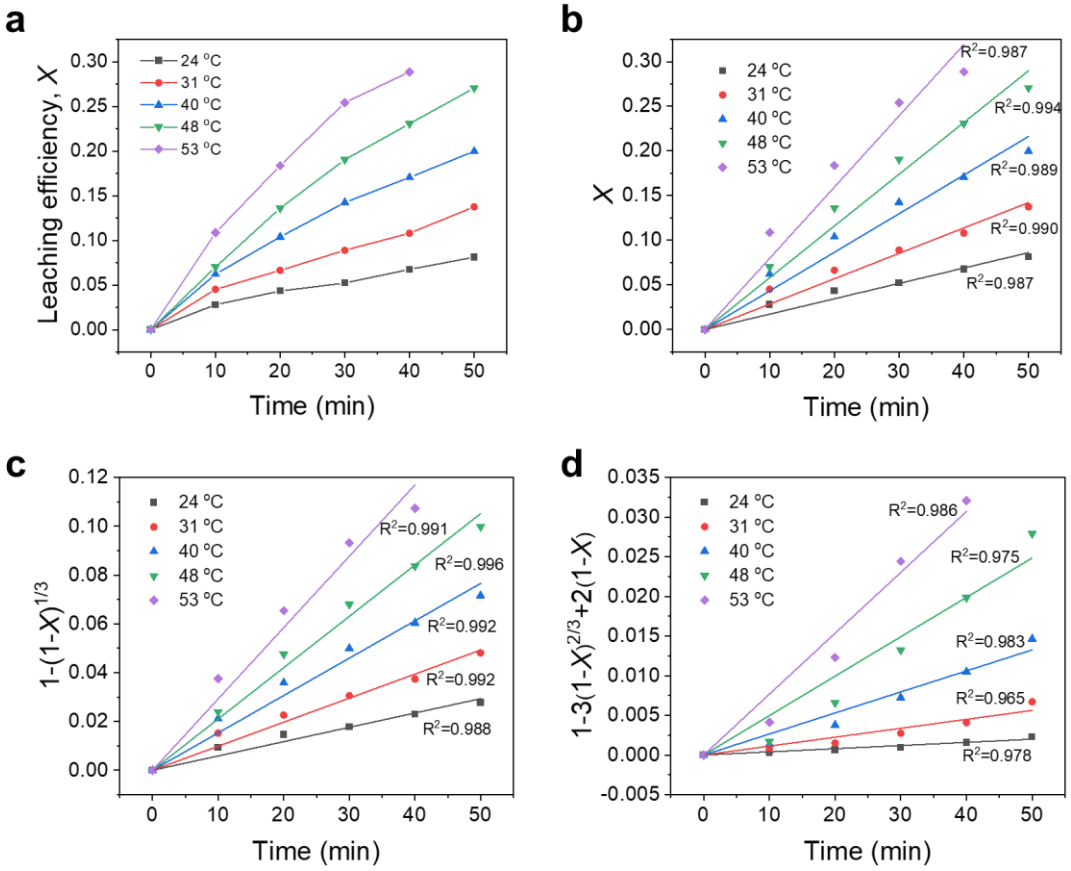

Figure S17. (a) Effects of temperature and time on the leaching efficiency of Mn from the commercially purchased NCM523 in 0.05 mol/L H_2SO_4 solution. Kinetics analysis for the Mn leaching from NCM523 under different reaction temperatures by (b) X vs. time, (c) $1-(1-X)^{1/3}$ vs. time, and (d) $1-3(1-X)^{2/3}+2(1-X)$ vs. time. The leaching kinetics of Mn from NCM523 was best fit with the surface chemical reaction control model in (c), based on the coefficients of determination (R^2).

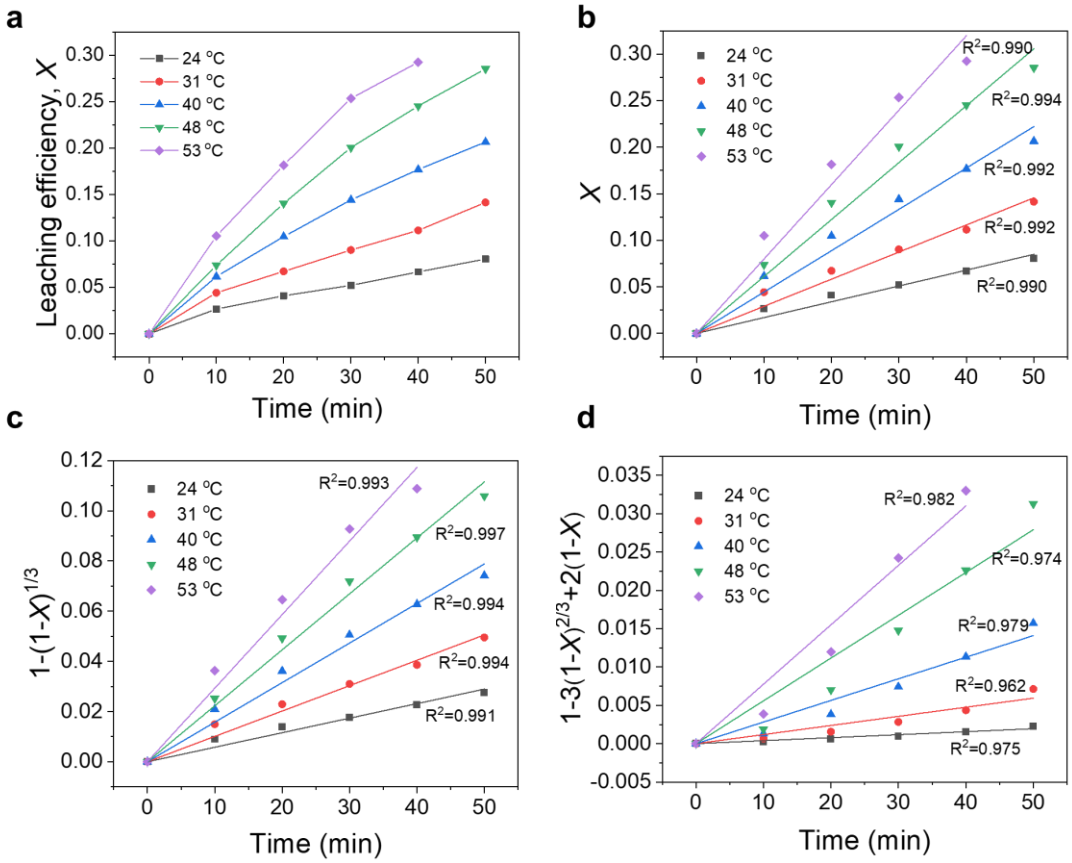

Figure S18. (a) Effects of temperature and time on the leaching efficiency of Ni from the commercially purchased NCM523 in 0.05 mol/L H_2SO_4 solution. Kinetics analysis for the Ni leaching from NCM523 under different reaction temperatures by (b) X vs. time, (c) $1-(1-X)^{1/3}$ vs. time, and (d) $1-3(1-X)^{2/3}+2(1-X)$ vs. time. The leaching kinetics of Ni from NCM523 was best fit with the surface chemical reaction control model in (c), based on the coefficients of determination (R^2).

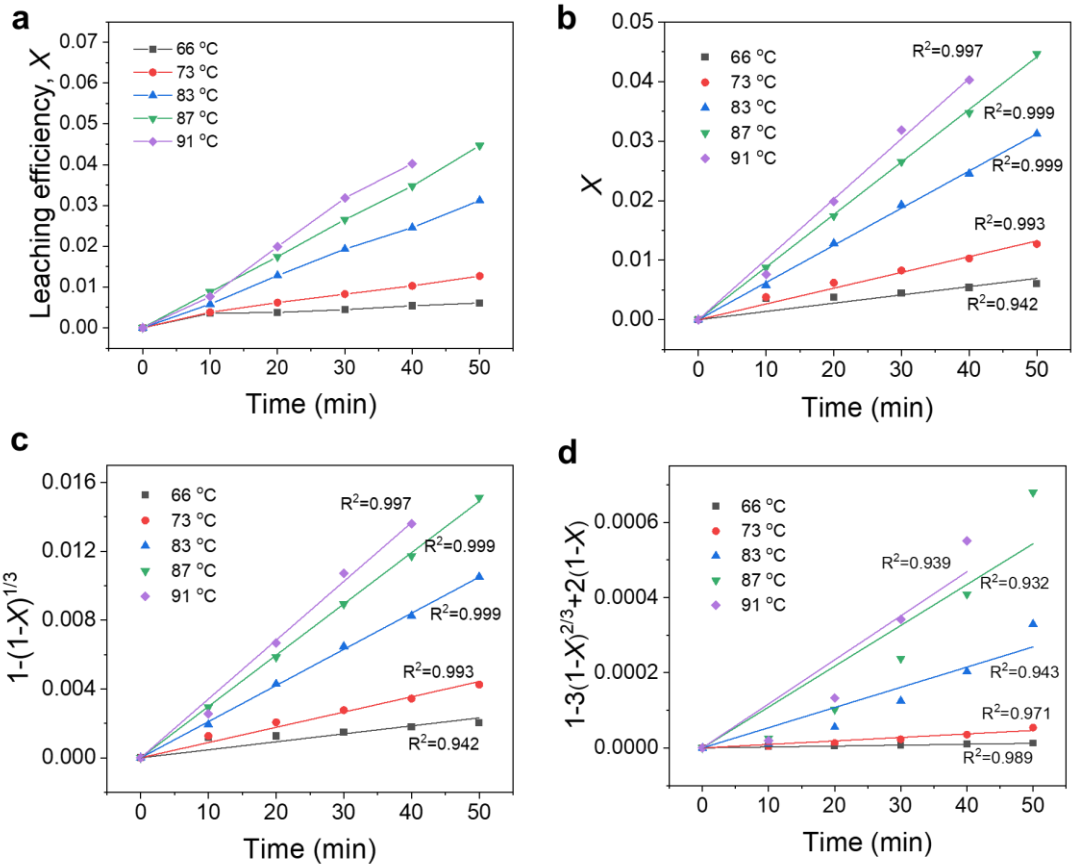

Figure S19. (a) Effects of temperature and time on the leaching efficiency of Ni from the commercially purchased NiO in 0.05 mol/L H_2SO_4 solution. Kinetics analysis for the Ni leaching from NiO under different temperatures by (b) X vs. time, (c) $1-(1-X)^{1/3}$ vs. time, and (d) $1-3(1-X)^{2/3}+2(1-X)$ vs. time. The leaching kinetics of Mn from $LiMn_2O_4$ was well fit with the surface chemical reaction control model in (c), based on the coefficients of determination (R^2) and the structural similarity of NiO to CoO and MnO.

Note S4. More discussion on the kinetics analysis for the leaching of transition metals from NCM523

It's worth mentioning that the use of one single model to fit the kinetics data may not grasp the complexity of the actual reaction. In addition to the surface chemical reaction control model (Figures S16c, S17c, and S18c), the leaching kinetics of Co, Mn, Ni also fit quite well with the residue layer diffusion control model (Figures S16d, S17d, and S18d). The values of the specific rate constant (k) obtained were used to plot new Arrhenius relationships. The activation energies for the leaching of Co, Mn, and Ni from NCM523 were determined to be 79, 80, and 81 kJ mol^{-1}, respectively. Although these values for Co, Mn, and Ni were greater than those in Figure 5C, the results still support the experimental finding that the transition metal elements are more easily leached from the roasted products than from the pristine cathode materials. Therefore, our conclusion on the critical role of H_2 reduction roasting is valid. In the future work, we will design and extend the kinetics experiments to the full dissolution process, to dig deep into the actual reaction mechanism that may be evolving or mixed with multiple rate-controlling steps during the leaching process.

References for Electronic Supplementary Information

1. A. Roine, *HSC Chemistry Database 5.11*, 2002, Outokumpu Research, Finland.
2. H. Sun and K. Zhao, *The Journal of Physical Chemistry C*, 2017, **121**, 6002-6010.
3. E. Billy, M. Joulié, R. Laucournet, A. Boulineau, E. De Vito and D. Meyer, *ACS Appl Mater Interfaces*, 2018, **10**, 16424-16435.